Optimal Allocation and Control of Superconducting Fault Current Limiter and Superconducting Magnetic Energy Storage in Mesh Microgrid Networks to Improve Fault Ride Through

A. Komijani, M. Kheradmandi, M. Sedighizadeh[*]

Department of Electrical Engineering, Shahid Beheshti University, Evin, Tehran, Iran.

Abstract- *Voltage drop during the fault can be effected on the performance of generation units such as wind turbines. The ability to ride through the fault is important for these generation units. Superconducting fault current limiter and superconducting magnetic energy storage can improve the fault ride through due to fault current limiting and voltage restoring ability during the fault, respectively. This paper presents a method for optimal allocation and control of superconducting magnetic energy storage and superconducting fault current limiters in meshed microgrids. For this purpose, the doubly-fed induction generator voltage deviation, the point of common coupling power deviation, the fault current of transmission lines, and superconducting fault current limiter and superconducting magnetic energy storage characteristics were considered as objective functions. In this paper, the optimization is performed in single-step and two-step by particle swarm optimization algorithm, and the system with the optimal superconducting magnetic energy storage and superconducting fault current limiters are analyzed and compared. The results of simulations show superconducting fault current limiter and superconducting magnetic energy storage reduce 85% of voltage drop, decreases 63% of doubly fed induction generator power deviation, and limits the maximum fault current of transmission lines by 9.8 pu. Finally, the status of the studied system variables has been investigated, in two scenarios related to the different fault locations with equipment that the optimal allocated.*

Keyword: Meshed Microgrid, superconducting fault current limiter, superconducting magnetic energy storage, Optimization.

NOMENCLATURE

c_1 to c_8	The coefficient of wind turbine power coefficient (-)
C_p	Wind turbine power coefficient (-)
E_{SFCL}	The SFCL energy losses during the fault condition (J)
E_{SMES}	The SMES capacity (J)
F_i	Maximum fault current of transmission lines (A)
F_p	The PCC power deviation (W)
F_v	The DFIG output voltage deviation (V)
i_{SFCL}	The SFCL current (A)
I_{SMES}	The SMES inductor current (H)
$I^l_{t_0-t_3}$	The transmission lines current during the fault (t_0 to t_3) (A)
K_{Pi}, K_{Ii}	The PI coefficients of SMES (-)
L_{SMES}	The SMES inductor (H)
R	The wind turbine radius (m)
R_m	The SFCL resistor at fault condition (Ω)
R_{SFCL}	The SFCL resistor vs time (Ω)
t_0	The fault occurring time (s)
t_1	The time of the SFCL resistor reaches R_m (s)
t_2	The fault clearing time (s)
t_3	The time of the SFCL resistor reaches zero (s)
t_s	The simulation time (s)
V_W	The wind velocity (m/s)
β	The pitch angle (º)
ΔP_{PCC}	The variation of PCC power (W)
ΔV_t	The variation of the DFIG output voltage (V)
λ	The tip speed ratio (-)
ρ	The air density (kg/m3)
τ_1	The time constants of SFCL resistor rising (s)
τ_2	The time constants of SFCL resistor falling (s)
ω_m	The angular velocity of the rotor (rad/s)

1. INTRODUCTION

The tendency for renewable energy as distributed energy resource (DER) is rising because of increasing energy consumption, reducing the reservoirs of

traditional energy resources and its environmental concerns. The connection of DER to the power system will lead to new topics, including their output power dependency on environmental conditions, the peak generation and consumption time mismatch, and issues related to the stability and protection of the system. The performance of some generation units, such as doubly-fed induction generators (DFIG), may be interrupted at low voltage levels. The capability to overcome a voltage drop or fault can prevent system interruptions, called Low voltage ride-through (LVRT) or fault ride-through (FRT).

The formation of microgrids has impaired conventional distribution system protection and affects the basic protection requirements, including sensitivity, correct selection, and speed [1]. Several methods for protecting the microgrid system have been proposed, which are divided into three main categories. The first category is distributed generation (DG) limitations that propose disconnecting DGs from the grid [2] or limiting the capacity of the DG [3]. This method is simple and doesn't need any upgrade in the protection system. However, the DG disconnecting or limitation may cause stability concerns [2] or DGs development restriction, respectively. The second category is applying the external devices that suggest some devices like the fault current limiter (FCL) [4] and the fault current source (FCS) [5] has been added to the grid for helping the microgrid protection system. Finally, the last category is modifying protection systems that recommend developing protection schemes like distance protection [6] and adaptive protection [7] schemes.

Several solutions have been suggested to improve the ability to overcome voltage drops during the fault. In [8], a control strategy has been presented for performance improvement of the photovoltaic (PV) inverters under the normal and the LVRT conditions. The authors studied all possible switching combinations and the current paths during the freewheeling period of the inverter. In the presented method, a reconfigurable pulse width modulation (PWM) method has been proposed to switch between two PWM methods so that it is providing better performance in the LVRT condition. Simulation results show the constant common-mode voltage and high efficiency can be achieved by the possible and appropriate switching combinations. In Ref. [9], a new single-phase transformerless grid-connected PV inverter has been presented. The suggested topology is based on maintaining the constant common-mode voltage to suppress the leakage current and to provide reactive

power injection capability during grid faults. The control strategies have been examined for injecting reactive power in the LVRT condition. The proposed inverter can generate a three-level and five-level output voltage. The FCL has been suggested due to the good performance in fault current limiting in some papers such as [10, 11]. In [12], a comparison was made between superconducting fault current limiter (SFCL) and Dynamic Voltage restorer (DVR) in low voltage conditions. The authors expressed DVR is more expensive than SFCL and overall, SFCL is considered the preferred option for improving LVRT.

FCL is an instrument that restricts the electric current without interruption by adding a resistor at the fault condition. SFCL is a special type of FCL that uses superconductors in this application, which is faster than the old one. The SFCL is always in the circuit, but in normal operation, it does not affect system performance, and when the fault occurs, the current is limited by the superconductor quenching and increasing the resistance. Other advantages of SFCL are included preventing the voltage drop, extending the life of other equipment, fast restoring after fault clearance, improving transient stability, and so on. Of course, SFCL alone can't compensate for the voltage drop and improve FRT. So, electrical energy storage such as superconducting magnetic energy storage (SMES) can be installed to ensure the power quality, operational flexibility, and transient stability of a microgrid.

The SMES has advantages such as high power density, fast charging speed [13], and long life [14], which made it a good choice for improving FRT in the network [15]. However, large SMES is needed because of the high current during the fault condition. In this case, the fault current limitation can be helpful. The existence of mesh in the system diagram has advantages such as increasing reliability, reducing voltage drop, and increasing the voltage level in the system. But the complexity of the protective issues of this structure has led to the almost distribution systems having a radial arrangement. So, most of the protection systems provided in the papers have been proposed for radial systems. The existence of the mesh makes the optimal allocation of various equipment complicated, such as protective equipment (like FCLs), and traditional methods are not efficient [16].

Several papers have been presented on the use of SFCL or SMES for protective objectives. The SFCL has been used in [12, 17]. The effect of FCL on DG development has been analyzed in [17] by considering

the coordination of relays. The weighted combination of the operating time of the primary overcurrent relays has been considered as the objective function. The results show that the fault current level has decreased below the allowable limit in different modes. On the other hand, the researchers recommended SMES to cross the fault in [15, 18]. The authors present a scheme for LVRT improvement of DFIG with SMES in [15]. The SMES is connected to the rotor side of DFIG. The SMES and rotor side converter have been controlled with two LVRT strategies. The results show that the proposed scheme can protect the key parameters of DFIG and enhance the grid voltage effectively under the LVRT condition [15]. Also, a control strategy has been proposed for a current source converter-based wind turbine-SMES hybrid system in Ref. [18]. The results show the hybrid system with the suggested control strategy has better operating performance on voltage dip conditions. Simultaneous use of SFCL and SMES is suggested in a few papers. In Ref. [19], the coordinated control of the flux coupling SFCL and SMES is provided to improve transient performance under fault conditions. The results of this paper show the fault current decreased, thus contributing to the improvement of the FRT. The method presented in this paper has been analyzed on a radial system. The aim of Ref. [20] is to optimize the superconducting coil inductance and the PI controller parameters to minimize the DFIG terminal voltage deviation and the power fluctuation during the fault. The results of this paper show that the maximum voltage drop of the DFIG bus has decreased, which indicates FRT improvement. The method presented in this paper has been investigated on the radial structure system. In Ref. [21], the optimal coordinated control of resistive-type SFCL and SMES is presented. In this paper, SMES is being chosen for power fluctuation damping after the fault. The control parameters were determined to minimize the loss of the SFCL resistor in the optimization section. The method presented in this paper is applied to a synchronous generator connected to a resistive load. Finally, in Ref. [22] authors provide coordinated control of UPFC with the SFCL and SMES for improvement of power system transient stability. The results show that SFCL solves the voltage drop of the SMES bus so that SMES able to help system stability. As the literature review is shown, SFCL and SMES improve network performance during the fault condition. In a few papers, simultaneous utilization of devices has been suggested. Also, the papers presented have studied simple structure systems, unlike practical systems.

In this paper, the optimal allocation and control of the superconducting fault current limiter and the superconducting magnetic energy storage device in a microgrid will be presented for improving the fault ride-through capability. First, the modeling of system components has been described. Then, the DFIG voltage deviation, the point of common coupling (PCC) power deviation, the fault current of transmission lines, and SFCL and SMES characteristics were considered as objective functions. The particle swarm optimization (PSO) algorithm will be used to optimize the objective functions. Finally, simulation results have been presented for the performance of the presented method. Finally, the innovations of the paper can be listed as follows:

- Improving the FRT in the microgrids including wind and PV through the use of SFCL and SMES
- Implementing the suggested method on the meshed microgrid
- Determining the optimal installation location of SFCL and SMES in the microgrid according to the objective functions
- Optimal determination of SFCL and SMES control specifications and control variables according to the objective functions.

2. MODELING OF SYSTEM COMPONENTS

In this paper, a method has been presented for optimal allocation and control of SFCL and SMES in a microgrid system that included wind and PV generation units, synchronous generator, and loads.

2.1. Distributed generators

The wind turbine generates electrical energy from the wind kinetic energy. The mechanical power of the wind turbine is obtained from Eq. (1).

$$P_{Wind} = \frac{\pi}{2} R^2 \rho C_p V_W^3 \qquad (1)$$

Where R is the radius of the wind turbine, ρ is the wind density, V_W is the velocity of the wind and C_p is the wind turbine power coefficient. The C_p depends on the tip speed ratio (λ) and the pitch angle (β), which is defined as Eq. (2).

$$C_p = c_1 \left(\frac{c_2}{\lambda_i} - c_3 \beta - c_4 \right) e^{\left(\frac{-c_5}{\lambda_i} \right)} + c_6 \lambda \qquad (2)$$

Where

$$\frac{1}{\lambda_i} = \frac{1}{\lambda + c_7 \beta} - \frac{c_8}{\beta^3 + 1} \qquad (3)$$

$$\lambda = \frac{\omega_m R}{V_W} \qquad (4)$$

Where ω_m is the angular velocity of the rotor and c_1 to c_8 is equal to 0.5176, 116, 0.4, 5, 21, 0.0068, 0.08, 0.035 [23].
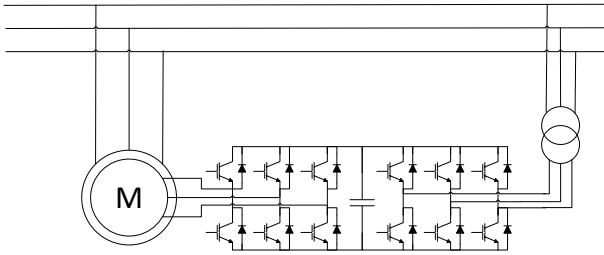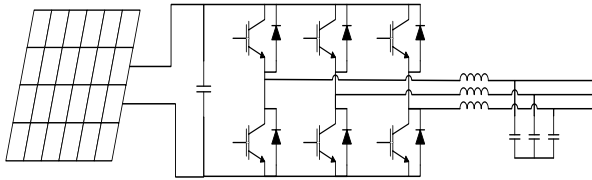
Fig. 1. The grid connection of the wind turbine
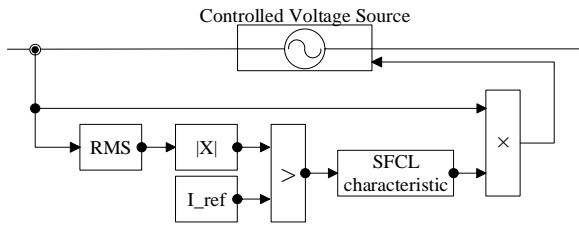

Fig. 2. The PV model

Fig. 3. The control diagram of the SFCL

The DFIG arrangement has been considered for connecting the wind turbine to the grid that the rotor has been connected to the grid via a back-to-back converter. The grid connection of the wind turbine is shown in Fig. 1. Similarly, the structure of PV has been presented in Fig. 2.

2.2. The SFCL

SFCL resistor has been considered zero and R_m at normal operation and fault condition, respectively. The SFCL shows zero resistance before the fault occurs. When the fault occurs, the superconductor starts to quench, and the SFCL resistor increases exponentially to steady-state value (R_m). When the fault clears, the superconductor return to superconducting mode and the SFCL resistor decreases exponentially to zero. So, the SFCL resistor has been considered as Eq. (5).

$$R_{SFCL}(t) = \begin{cases} 0 & t < t_0 \\ R_m\left(1 - e^{\left(\frac{-t}{\tau_1}\right)}\right) & t_0 < t < t_1 \\ R_m & t_1 < t < t_2 \\ R_m\left(e^{\left(\frac{-t}{\tau_2}\right)}\right) & t_2 < t < t_3 \\ 0 & t > t_3 \end{cases} \quad (5)$$

Where t_0 is the time of the fault occurring, t_1 is the time the SFCL resistor reaches R_m, t_2 is the time of fault clearing and t_3 is the time the SFCL resistor reaches zero. Also, τ_1 and τ_2 are the time constants of the rising and falling of the SFCL resistor during the fault, respectively. The value of R_m will be calculated by

optimizing the objective function in the next sections. The time constant values (τ_1 and τ_2) are assumed to be 0.01 and 0.1 seconds, respectively. t_0 and t_2 will be considered 1 and 1.2 seconds in the simulation result section. According to the property of exponential functions, the value reaches almost the steady-state after fivefold of the time constant ($5 \times \tau$). So, t_1 and t_3 are obtained 1.05 and 1.7 seconds.

The control diagram of the SFCL is presented in Fig. 3. First, the current is measured and the RMS of the current is calculated. Then, the RMS current is compared with the fault current reference (I_ref). If the RMS current exceeds the reference value, the SFCL characteristic block provides the resistance value based on Eq. (5) at its output. Finally, SFCL was modeled as a variable resistor using a voltage source dependent on the value obtained from Eq. (5).

2.3. The SMES

Enormous energy can be stored in the Electromagnetic field by using the superconductors in the inductor. The superconducting inductor has been connected to a DC link via a DC chopper. An AC/DC converter feeds the DC link from the AC grid. The SMES structure is shown in Fig. 4.

The control diagram of the chopper is considered as Fig. 5. In this paper, two modes have been assumed to control SMES including discharge and stand-by mode. In normal conditions, the standby mode is active, where the inductor current flows through the S1 and the D2. So, the SMES current remains constant. In the fault condition, the discharge mode will activate, and the inductor current is discharged in the capacitor through the D1 and the D2. The rate of the inductor discharge depends on the duty cycle of the S1. The gate of S1 is controlled by the power of the DFIG. Also, S2 will be applied in charging mode that inductor current charges through the S1 and S2. This algorithm has been adapted from [24]. In the VSC converter, the DC-link has the same polarity consistently and the bidirectional power flow is achieved by changing the DC current direction. The control diagram of the VSC converter is considered as Fig. 6. In this structure, the power flow through the VSC converter has been controlled by DC voltage and DFIG voltage and power in the dqo-domain.
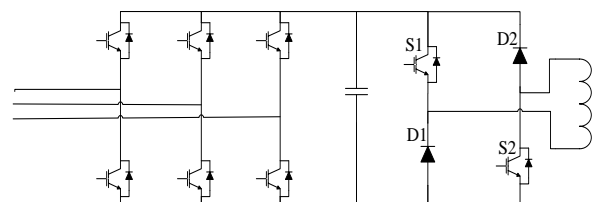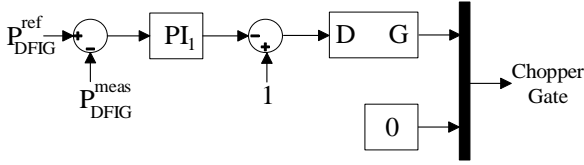

Fig. 4. The SMES structure
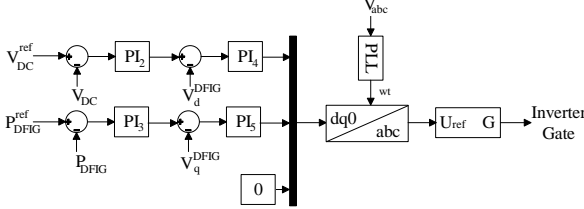
Fig. 5. The control diagram of the chopper

Fig. 6. The control diagram of the SMES inverter

3. OBJECTIVE FUNCTIONS

In this paper, a method has been presented for optimal allocation and control of SFCL and SMES in the microgrid to improve the system performance at fault conditions. So, five objective functions are considered that will be used in optimizations.

1. The DFIG output voltage deviations:

Fault cause voltage drop around the fault location, which leads to problems such as the instability of wind units. So it is important to investigate the DFIG output voltage deviations by Eq. (6).

$$F_v = \sqrt{\int_0^{t_s} (\Delta V_t)^2 \, dt} \qquad (6)$$

Where t_s is the simulation time and ΔV_t is the variation of the DFIG output voltage in pu.

2. The PCC power deviations:

Due to high power density, the SMES has a significant effect on power fluctuation reduction. Power fluctuations may harm the system components which show its importance. Eq. (7) presents PCC power deviations.

$$F_p = \sqrt{\int_0^{t_s} (\Delta P_{PCC})^2 \, dt} \qquad (7)$$

Where ΔP_{PCC} is the variation of PCC power.

3. The Maximum fault current of distribution lines:

Fault current limiting can help improve the FRT. The fault current of transmission lines varies due to the mesh grid structure. So, the Maximum fault current of transmission lines in pu has been considered as an objective function obtained by Eq. (8).

$$F_i = \max_l \left(I_{t_0-t_3}^l \right) \qquad (8)$$

Where $I_{t_0-t_3}^l$ is the current of transmission lines during the fault (t_0 to t_3).

4. The SFCL energy losses:

Electrical energy wastes in SFCL resistor due to current limitation. As the number or resistance of the SFCL increases, the microgrid performance improves during the fault condition, but the cost and energy losses of SFCL increase. Therefore, it is important to evaluate the SFCL energy losses during the fault condition, by Eq. (9).

$$E_{SFCL} = \int_{t_0}^{t_3} R_{SFCL} i_{SFCL}^2 \, dt \qquad (9)$$

Where i_{SFCL} is the current of the SFCL.

5. The SMES capacity:

SMES capacity has a remarkable impact on the power injected into the grid at the fault condition for compensating the voltage drop and the FRT. As the SMES capacity increases, the voltage drop compensation will be increased and FRT will improve. But greater SMES capacity increase costs. So, the SMES capacity is considered as an objective function calculated from Eq. (10).

$$E_{SMES} = \frac{1}{2} L_{SMES} I_{SMES}^2 \qquad (10)$$

Where L_{SMES} is the inductor of SMES and I_{SMES} is the current of SMES inductor.

6. Main objective functions:

In this paper, an optimization problem has been solved to determine the location of SMES and SFCL, the inductance of SMES, the SFCL resistor, and control parameters. Two cases have been considered to solve the optimization problem. In the first case, the optimization has been done in two steps. First, the SFCL resistor, SMES inductor, and their locations are determined by Eq. (11). Then, the control parameters are determined by Eq. (12). Fig. 7 shows the algorithm of SMES and SFCL allocation in the first case.

$$Min \, F_1 = \omega_3 \hat{F}_i + \omega_4 \hat{E}_{SFCL} \qquad (11)$$
$$Min \, F_2 = \omega_1 \hat{F}_V + \omega_2 \hat{F}_p + \omega_5 \hat{E}_{SMES} \qquad (12)$$

In the second case, all parameters are determined in one step by Eq. (13). Fig. 8 shows the algorithm of SMES and SFCL allocation in the second case.

$$Min \, F = \omega_1 \hat{F}_V + \omega_2 \hat{F}_p + \omega_3 \hat{F}_i + \omega_4 \hat{E}_{SFCL} + \omega_5 \hat{E}_{SMES} \qquad (13)$$

Where variable with hat accent is normalized variable. Constraints of the problem in both cases, include:

- Inductance of SMES: $0 < L_{SMES} < 10H$
- SFCL resistor: $0 < R_m < 10\Omega$
- PI coefficients: $0.1 < K_{Pi}, K_{Ii} < 10$
- Location of SMES: on buses
- Location of SFCL: PCC, middle and ends of lines.

In this paper, the studied system has been implemented in Simulink and conjoined with the

developed PSO algorithm in Matlab. As shown in the algorithm of Fig. 7 and 8, the desired parameters are determined in the form of a particle in the PSO algorithm and defined as the input of the model. After simulating the model, the values of the objective functions are calculated with the same coefficients. Then, new particles are defined. This process continues until the objective function is optimized. The value of the discrete parameter is corrected and rounded in determining new particles.
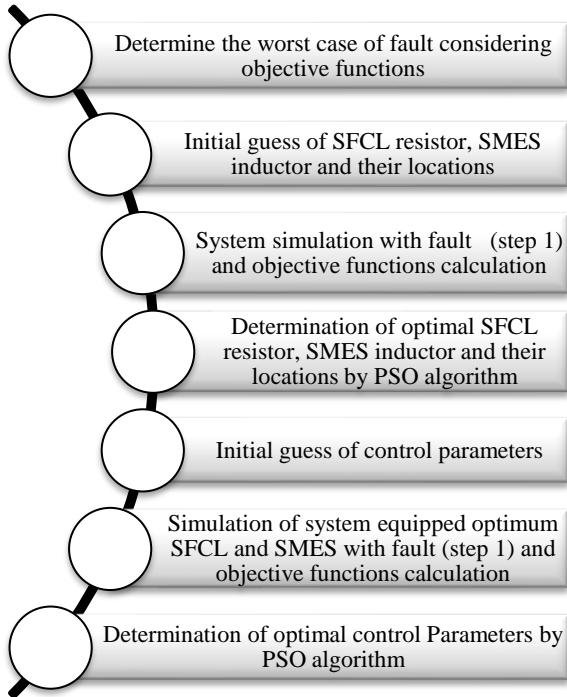

Fig. 7. the algorithm of SMES and SFCL allocation in two-step optimization
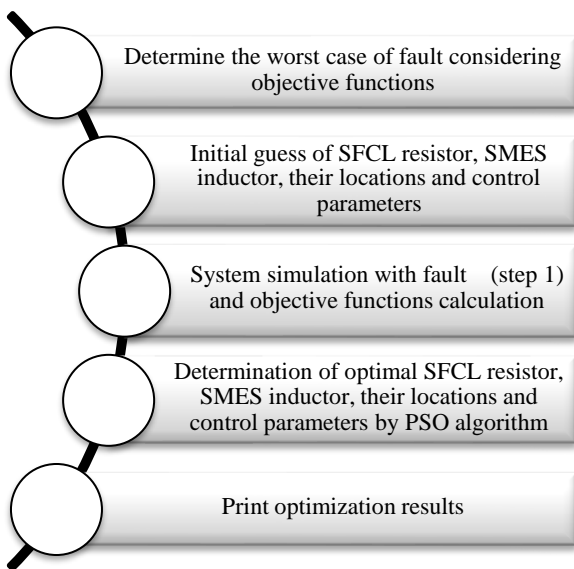
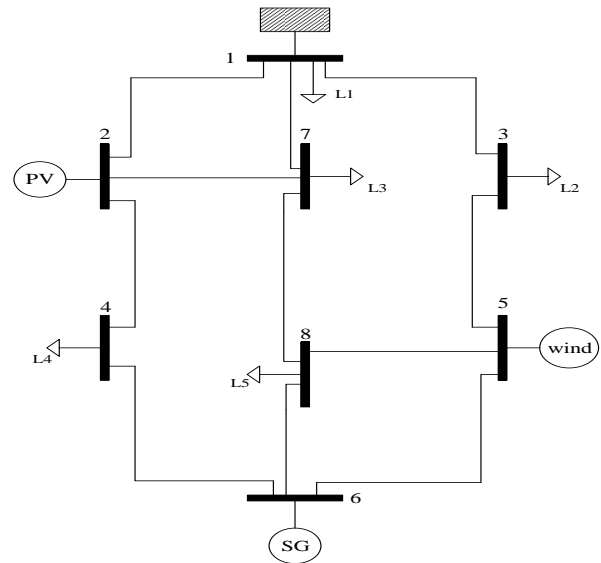**Fig. 8. the algorithm of SMES and SFCL allocation in single-step optimization**

Fig. 9. the structure of the system studied

Table 1. The microgrid and its components parameters

Main Network System	
PV	150kW
wind	350kW
SG	500kW
Equivalent power source	10 kV/50 Hz
Load	
L1	(130+j15)kVA
L2	(300+j25)kVA
L3	(100+j10)kVA
L4	(170+j20)kVA
L5	(400+j60)kVA
Transmission line (0.1+j0.4 Ω/km)	
$l_{17}, l_{24}, l_{35}, l_{68}$	10 km
l_{27}, l_{58}, l_{78}	15 km
$l_{12}, l_{13}, l_{46}, l_{56}$	20 km

4. SIMULATION RESULT

In this paper, the system studied is a 10 kV microgrid. The microgrid includes the wind and PV units, synchronous generator, and loads. The microgrid arrangement is presented in Fig. 9. It is clear that some meshes exist in the microgrid and its structure is more complicated. The microgrid and its component parameters are indicated in Table 1. The simulations are carried out under a temporary three-phase fault at t=1s for 200 milliseconds.

4.1. Base case:

The cognition of the present state of the system is important in optimizing the process and comparing the results. In this section, the system studied is simulated without any additional equipment. Then, the objective functions have been calculated. These will be used to normalize the objective functions in the optimization process.

The worst case of faults in microgrids is needed in the optimization process. For this purpose, the studied system is simulated considering the three-phase fault at the beginning, middle, and end of transmission lines without any additional equipment. The objective functions have been obtained in each case. Finally, the objective functions have been normalized and presented as Fig. 10. As it can be seen, the worst case of faults in the microgrid is in case #19 which is related to the fault in bus number 7. This selection is justified because of the centrality of the bus in the microgrid topology.

4.2. Two-step optimization
Determining parameters by optimizing the objective functions that are most relevant to them may yield better results. Also, the two-step allocation can reduce computational load. The characteristics and location of the SMES and SFCL in the system studied have been determined by optimizing the objective functions presented in Eq. 11 and 12 according to the algorithmic procedure of Fig. 7. After executing the optimization, the optimal values of the SFCL and SMES parameters are obtained in Table 2.

4.3. Single-step optimization
Determining parameters by optimizing a global objective function can lead to the global optimal point and the result is more appropriate. It does, however, impose more computational load. The characteristics and location of the SMES and SFCL in the system studied have been determined optimizing the objective function presented in Eq. 13 according to the algorithmic procedure of Fig. 8. After executing the optimization, the optimal values of the SFCL and SMES parameters are obtained in Table 3.

The system studied with the SMES and SFCL allocated in two optimization cases will be compared with the base case to show the impact of SMES and SFCL during the fault time. The DFIG bus Voltage for Different cases is presented in Fig. 11. As it can be seen, the bus voltage drops to 0.18 pu during fault time, but the voltage drop decreased 73 and 85 percent with SMES and SFCL for cases one and two, respectively. Simultaneous application of SFCL and SMES has been able to completely improve the DFIG voltage status. The difference between optimization modes is the DFIG voltage level during the fault, which the single-step optimization has better behavior. Also, the PCC power for the above cases is presented in Fig. 12. In this figure, it is clear that the PCC power growth in fault time has decreased by SMES and SFCL 56% and 63% for cases one and two, respectively. As it is presented, the PCC power has improved with the presence of SFCL and SMES in both optimization modes, which the result of

single-step optimization is better.

Table 2. optimized parameters of SMES and SFCL in two-step optimization

Parameters	Value
SFCLs location	The bottom end of l_{17}, l_{78}, and l_{46}
R_m	8.491 Ω
SMES location	Bus 5
L_{SMES}	6.743 H
I_{SMES}	1.136 kA
K_{p1}, K_{i1}	3.715, 2.491
K_{p2}, K_{i2}	1.937, 3.764
K_{p3}, K_{i3}	1.702, 2.844

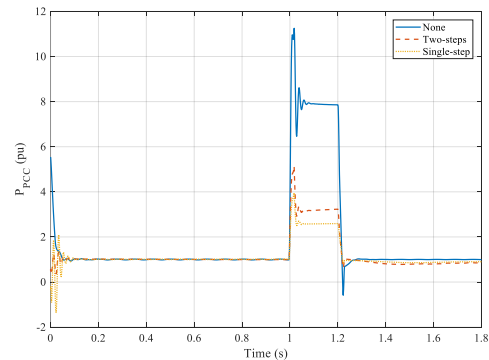**Table 3. optimized parameters of SMES and SFCL in single-step optimization**

Parameters	Value
SFCLs location	The bottom end of l_{17}, l_{78}, and l_{13}
R_m	7.625 Ω
SMES location	Bus 8
L_{SMES}	5.314 H
I_{SMES}	1.172 kA
K_{p1}, K_{i1}	4.529,3.161
K_{p2}, K_{i2}	2.393,4.824
K_{p3}, K_{i3}	1.367,3.278
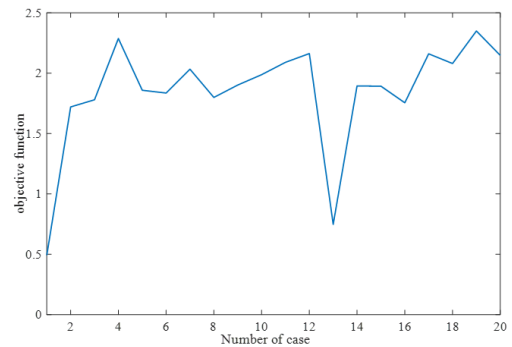
Fig. 10. the objective functions considering faults
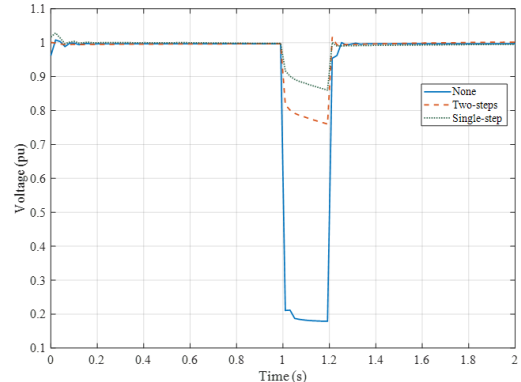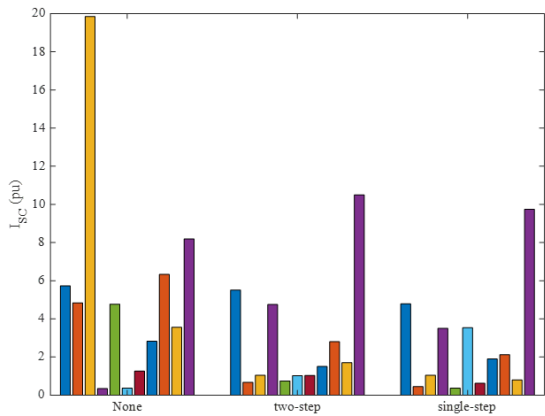

Fig. 11. The DFIG bus Voltage

12. The PCC output power

Table 4. SFCL energy losses and SMES capacity

Parameters	Two-step	Single-step
E_{SFCL} (MJ)	5.834	4.671
E_{SMES} (MJ)	4.3509	3.6496

Fig. 13. Transmission line fault current

The maximum fault current of the transmission lines is another important parameter considered in this paper. The fault current of the transmission lines in three cases is shown in Fig. 13. As a result of the optimizations, the fault current in the system studied is limited to 10.2 and 9.8 pu, which is reduced in the amount of 48.7 and 48.96 percent for cases one and two, respectively. The fault current of most transmission lines has decreased by the presence of SFCL and SMES, and the maximum transmission line error has also decreased. The energy losses in the SFCL during fault time and the SMES capacity allocated in two cases are presented in Table 4. The result shows the SFCL energy losses and the SMES capacity are higher in single-step optimization, which means higher economic costs, also.

The presented results show that the designed equipment has almost the same effect on the reduction of voltage and PCC power fluctuations and fault current, but the equipment designed in the single-step optimization has fewer capacity and loss. So, the allocation obtained from the single-step optimization is considered as the final allocation of SMES and SFCL and its control. The status of the studied system variables has been investigated, in two scenarios related to the different fault locations with equipment that the optimal allocated.

### 4.4. Scenario 1: fault in bus #7

In the first scenario, the symmetrical three-phase fault occurs on bus 7. The fault occurs at 1sec during 0.2 sec. The system under study will be tested in four different modes, including no equipment, with SFCL, with SMES, and finally with the simultaneous use of SFCL and SMES.

The voltage of buses #2 and #5 as the output nodes of the wind and solar generation units affect their performance, as shown in Fig. 14. The presence of SFCL

reduces the output voltage drop of PV and wind during the fault. The use of SMES also had a more positive effect on voltage drop. Finally, the simultaneous use of both of this equipment has been able to minimize the voltage drop during the fault, and thus it has helped the system under study to pass the fault. Also, Fig. 15 shows the diagrams of the external grid, PV power, and wind power in a, b and c, respectively. As shown in the figure, the presence of SFCL reduces the grid injection power during the fault. Also, SFCL has been able to reduce the power generation drop of the wind and PV units. The SMES has also had lower positive effects. Finally, the simultaneous use of both devices has been able to further improve the performance of the system during the fault, and the FRT capability of the system has been increased.
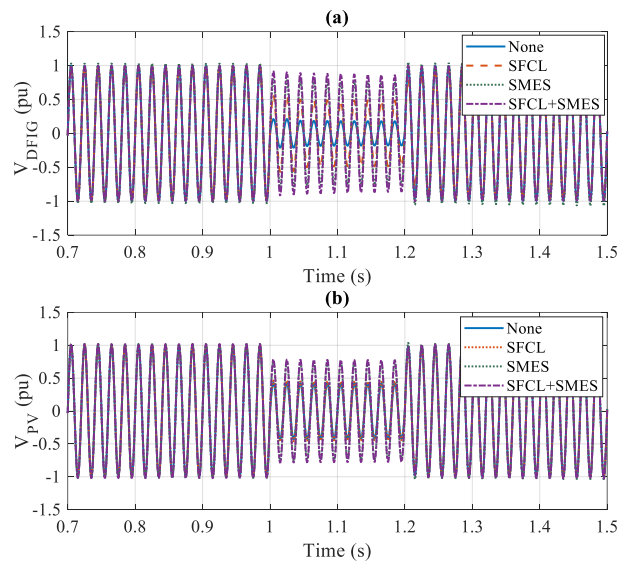
Fig. 14. Output voltage diagram of (a) DFIG (b) PV in scenario 1
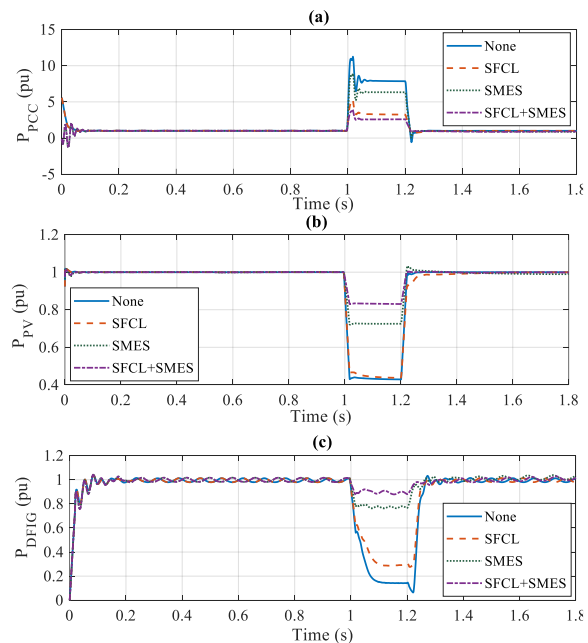
Fig. 15. Diagram of (a) P_{PCC} (b) P_{PV} (c) P_{DFIG} in the scenario 1

Fig. 16 presents the diagram of the electromagnetic torque and rotor speed of the DFIG to clarify the DFIG status during the fault. Based on these results, SMES had a greater effect on the electromagnetic torque and rotor speed during the fault than SFCL. Finally, SFCL and SMES have been able to achieve more stable DFIG performance during the fault.

As explained, SMES has been able to assist the system in overcoming the fault. Fig. 17 shows the power injection of SMES into the system in the lone SMES and SFCL with SMES. As it can be seen, more power is injected when SMES is used alone, but the most favorable result is obtained when using both SFCL and SMES. This indicates the Necessity of SFCL and SMES deploying simultaneously for such applications.
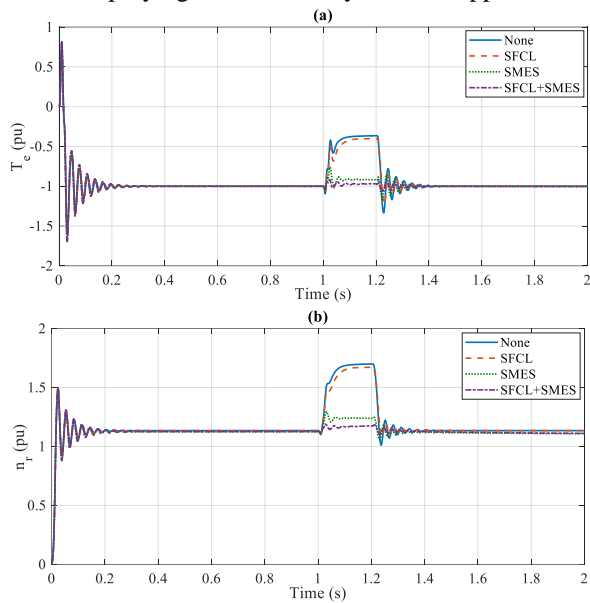

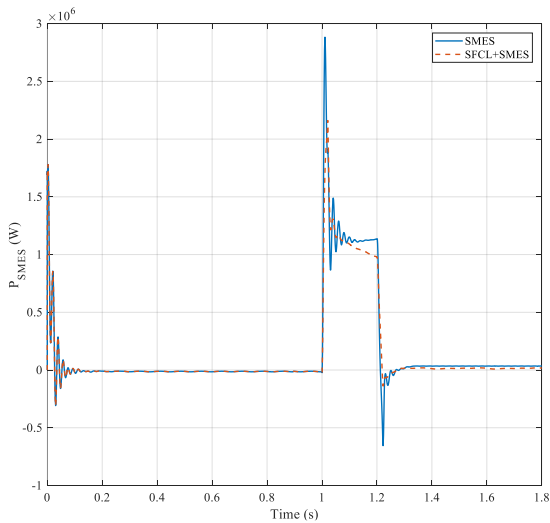Fig. 16. The diagrams of (a) electromagnetic torque (b) rotor speed of DFIG in scenario 1

Fig. 17. Diagram of P_{SMES} in scenario 1

The SFCL is responsible for limiting fault current.

Fig. 18 shows the maximum fault current of the transmission lines. As it can be seen, the presence of SFCL reduces the maximum fault current. Also, SFCL changes the current flow direction in the system causing the result difference in four cases. However, the injection of current by SMES into the grid has caused a slight increase in the maximum fault current.

4.5. Scenario 2: fault in the middle of the transmission line between bus #5 and #6

In the second scenario, the symmetrical three-phase fault occurs in the middle of the transmission line between bus #5 and #6. The simulation assumes are similar to the first scenario. The output voltage of the wind and solar generation units has been presented in Fig. 19. In this scenario, the SMES has a positive effect on voltage drop, but the SFCLs didn't help voltage drop. Finally, SFCLs and SMES passed the system through fault. Also, Fig. 20 shows the diagrams of the external grid, PV power, and wind power in a, b and c, respectively. As it can be seen in the figure, the status of PV and external grid power in the second scenario are better than in the first scenario. But DFIG performance was better in the first scenario. Finally, SMES and SFCL help the system at fault ride through.
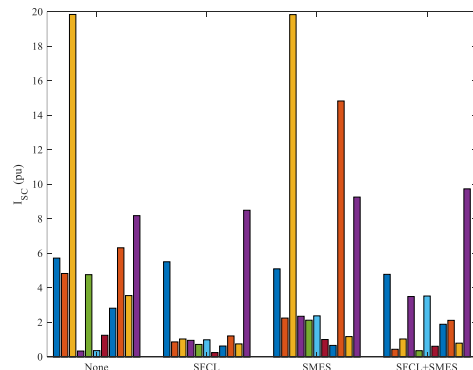

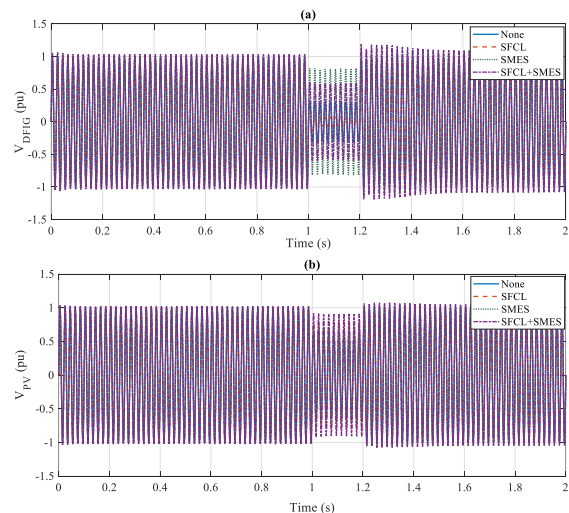Fig. 18. The maximum fault current of the transmission lines in scenario 1

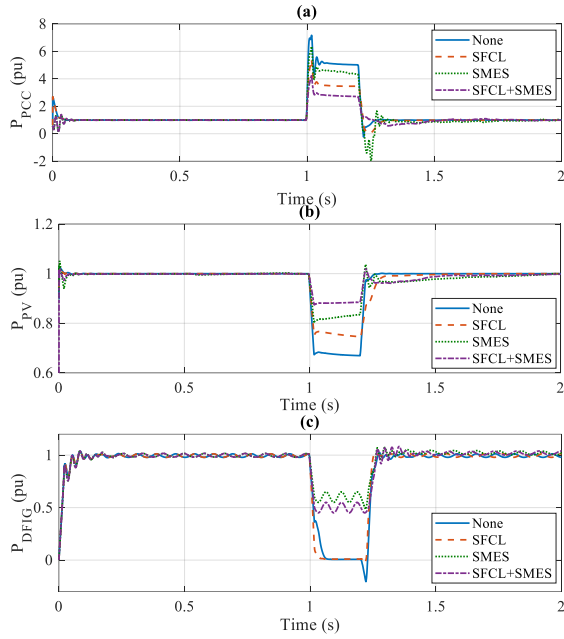Fig. 19. Output voltage diagram of (a) DFIG (b) PV in scenario 2

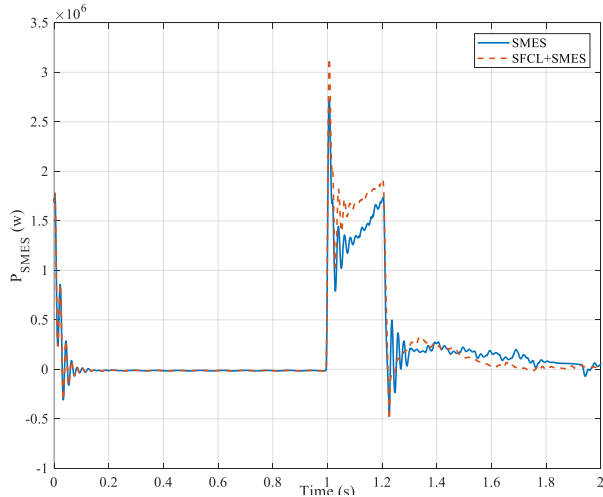**Fig. 20. Diagram of (a) P_PCC (b) P_PV (c) P_DFIG in scenario 2**

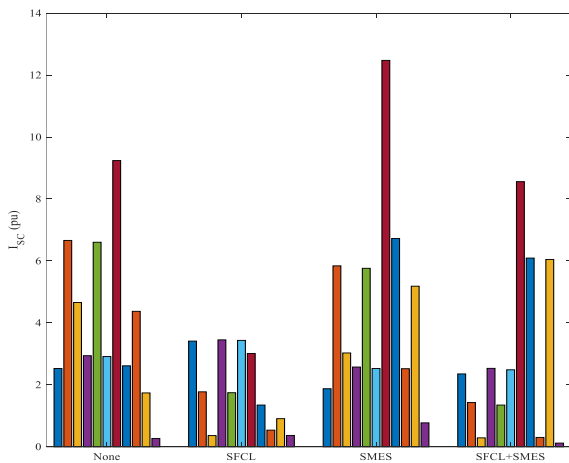**Fig. 21. Diagram of _PSMES_ in scenario 2**

Fig. 22. The maximum fault current of the transmission lines in scenario 2

As explained, SMES has been able to assist the system in overcoming the error. Fig. 21 shows the power

injection of SMES into the system in the alone SMES and SFCL with SMES. As it can be seen, similar to the previous scenario, more power was injected when SMES was used alone. Finally, Fig. 22 shows the maximum fault current of the transmission lines. As it can be seen, same as in the previous scenario, the presence of SFCL has reduced the maximum fault current. However, the injection of current by SMES into the grid has caused a slight increase in the maximum fault current. Also, the fault current level is lower in this scenario due to fault location.

5. CONCLUSION

The purpose of this paper was the optimal allocation and control of SMES and SFCL in the meshed microgrid to improve the fault ride-through capability. Some objective functions were defined, and optimization was described in single-step and two-step. The procedure was implemented on a meshed microgrid with solar and wind units and a synchronous generator. The simulation results were presented in two scenarios and compared. Finally, the optimal allocation and control of SFCL and SMES reduce 85% of voltage drop, decrease 63% of power fluctuations and limit the maximum fault current of transmission lines by 9.8 pu. Also, the status of the studied system variables has been investigated, in two scenarios related to the different fault locations with equipment that the optimal allocated. The results of the scenarios show that allocated SFCL and SMES improve the microgrid behavior during the fault at different fault locations and FRT capability is improved. In the future, by considering the literature review and simulation result of this paper, it is proposed to study a SMES controller for soft mode switching.

Appendix A.

Table A.1. Additional technical data

External grid	
Nominal Voltage (L-L, RMS)	10 kV
Frequency	50 Hz
PV	
Nominal Power	150 kW
Short circuit current	318.6 A
Open circuit voltage	569.8 V
PV transformer ratio	400V/10kV
Wind	
Nominal Power	350kW
Nominal voltage	1KV
Frequency	50Hz
Pole Number	4
Base wind speed	12m/s
Wind transformer ratio	1kV/10kV

REFERENCES

[1] N. Mohamed, M. Salama., "A review on the proposed solutions to microgrid protection problems", *Proc. CCECE*, 2016.

[2] North America Electric Reliability Corporation (NERC), "Performance of Distributed Energy Resources During and After System Disturbance Voltage and Frequency Ride-Through Requirements", *A report by the Integration of Variable Generation Task Force* (Task 1-7), 2013.

[3] H. Zhan et al., "Relay protection coordination integrated optimal placement and sizing of distributed generation sources in distribution networks", *IEEE Trans. Smart Grid*, vol. 7, pp. 55-65, 2016.

[4] U. Khan et al., "Application and positioning analysis of a resistive type superconducting fault current limiter in AC and DC microgrids using simulink and simpowersystem", *Proc. 1ˢᵗ ICEPE-ST*, 2011.

[5] F. Overbeeke, "Fault current source to ensure the fault level in inverter-dominated networks", *20ᵗʰ CIRED*, 2009.

[6] W. Huang et al., "An impedance protection scheme for feeders of active distribution networks", *IEEE Trans. Power Del.*, vol. 29, pp. 1591-1602, 2014.

[7] H. Laaksonen, D. Ishchenko, and A. Oudalov, "Adaptive protection and microgrid control design for hailuoto island", *IEEE Trans. Smart Grid*, vol. 5, pp. 1486-93, 2014.

[8] M. Farhadi-Kangarlu, F. Mohammadi, "Performance improvement of single-phase transformerless grid-connected PV inverters regarding common-mode voltage (CMV) and LVRT", *J. Oper. Autom. Power Eng.*, vol. 7, pp. 1-15, 2019.

[9] F. Mohammadi et al., "Design of A single-phase transformerless grid-connected PV inverter considering reduced leakage current and LVRT grid codes", *J. Oper. Autom. Power Eng.*, vol. 9, pp. 49-59, 2021.

[10] S. Blair et al., "Analysis of energy dissipation in resistive superconducting fault-current limiters for optimal power system performance", *IEEE Trans. App. Supercond.*, vol 21, pp. 3452-57, 2011.

[11] S. Faried, and M. Elsamahy, "Incorporating superconducting fault current limiters in the probabilistic evaluation of transient recovery voltage", *IET Gen., Trans. Dist.*, vol 5, pp. 101-107, 2011.

[12] C. Lei et al., "Comparison of superconducting fault current limiter and dynamic voltage restorer for LVRT improvement of high penetration microgrid", *IEEE Trans. App. Supercond.*, vol. 27, pp. 1-7, 2017.

[13] T. Nakayama et al., "Micro power grid system with SMES and superconducting cable modules cooled by liquid hydrogen", *IEEE Trans. App. Supercond.*, vol. 19, pp. 2062-5, 2009.

[14] M. Molina and P. Mercado, "Power flow stabilization and control of microgrid with wind generation by superconducting magnetic energy storage", *IEEE Trans. Power Elec.*, vol. 26, pp. 910-922, 2011.

[15] X. Xiao et al., "Cooperative rotor-side SMES and transient control for improving the LVRT capability of grid-connected DFIG-based wind farm", *IEEE Trans. App. Supercond.*, vol. 29, pp. 1-5, 2019.

[16] P. Yu et al., "Optimal location and sizing of fault current limiters in mesh networks using iterative mixed integer nonlinear programming", *IEEE Trans. Power Syst.*, vol. 31, pp. 4776-83, 2016.

[17] Y. Kim, H. Jo, and S. Joo, "Analysis of impacts of superconducting fault current limiter (SFCL) placement on distributed generation (DG) expansion", *IEEE Trans. App. Supercond.*, vol. 26, pp. 1-5, 2016

[18] Z. Wang et al., "Improvement of operating performance for the wind farm with a novel CSC-Type wind turbine-SMES hybrid system", *IEEE Trans. Power Del.*, vol. 28, pp. 693-703, 2013.

[19] C. Lei et al., "Coordinated control of SFCL and SMES for transient performance improvement of microgrid with multiple DG units", *Canadian J. Elect. Comp. Eng.*, vol. 39, pp. 158-67, 2016.

[20] I. Ngamroo, "Optimization of SMES-FCL for augmenting FRT performance and smoothing output power of grid-connected DFIG wind turbine", *IEEE Trans. App. Supercond.*, vol. 26, pp. 1-5, 2016.

[21] R. Rajashekar et al., "Coordinated control of optimized SMES and SFCL for the improvement of power system transient stability", *Proc. ICEEOT*, 2016.

[22] R. Stalin, S. Senthil Kumar, and K. Fathima, "Coordinated control of UPFC with SMES and SFCL for improvement of power system transient stability", *Proc. Sec. ICONSTEM*, 2016.

[23] S. Heier, "Grid integration of wind energy: onshore and offshore conversion systems", *John Wiley & Sons Ltd*, 2014

[24] F. Noorolah, S. Soleymani, F. Faghihi, "Voltage sag investigation of microgrid in the presence of SMES and SVC", *Sig. Proc. Renew. Eng.*, vol. 3, pp. 23-34, 2019.